Research Square

Preprints are preliminary reports that have not undergone peer review.
They should not be considered conclusive, used to inform clinical practice,
or referenced by the media as validated information.

Catalpol attenuates renal injury by regulating oxidative stress and inflammation response

Zhihui Liu
Northeast Agricultural University
Yu Wang
Northeast Agricultural University
Chong Zhou
Northeast Agricultural University
Qingyang Xu
Northeast Agricultural University
Hongxin Gao
Northeast Agricultural University
Mohan Huo
Northeast Agricultural University
Xiaowen Jiang
Northeast Agricultural University
Wenhui Yu (yuwenhui@neau.edu.cn)
Northeast Agricultural University

Research Article

Keywords: Catalpol, Aristolochic acid I, Renal injury, Oxidative stress, Inflammation, Apoptosis

Posted Date: December 14th, 2022

DOI: https://doi.org/10.21203/rs.3.rs-2361422/v1

License: This work is licensed under a Creative Commons Attribution 4.0 International License.
Read Full License

Abstract

Background: Aristolochic acid I (AA-I) can damage the structure and function of kidney, but there are few prevention strategies at present. In this study, we investigated the protective effects and mechanism of Rehmannia glutinosa extract-catalpol (CAT) on renal injury caused by AA-I.

Methods: In vitro, NRK-52E cells were administered with AA-I (40 μM) or/and CAT (10 μM, 5 μM) for 24 h. In vivo, C57BL/6NJ male mice were administered with AA-I (10 mg/kg) or/and CAT (100 mg/kg, 10 mg/kg) for 28 d. Clinical symptoms, histopathology, Elisa, quantitative RT-PCR, Westernblot, immunocytochemistry, immunofluorescence and flow cytometry were used to evaluate the protective effect of CAT on renal injury.

Results: In the model group, the body weight and renal function of mice decreased significantly, and the pathological damage of renal tissue was obvious. Compared with the model group, CAT can significantly improve the kidney structure and function. Activate NF-E2-related-factor-2 (Nrf2) signal pathway, increase antioxidant enzyme activity and decrease ROS and MDA levels. CAT can also inhibit the nuclear-factor-kappa-B (NF-κB) signaling pathway and reduce the expression of Cyt-c, TNF-α and pro-IL-1β. In addition, CAT can reduce Ca^{2+} concentration, endoplasmic reticulum (ER) stress and mitochondrial damage, thus reducing mitochondrial pathway apoptosis and cell apoptosis rate. And both Nrf2 and NF-κB are the main targets of CAT in alleviating AA-I-induced renal injury.

Conclusion: CAT can attenuate the damage of renal structure and function through Nrf2/NF-κB pathways. CAT can inhibit inflammation and oxidative stress, further reducing the mitochondrial pathway apoptosis and endoplasmic reticulum stress pathway apoptosis.

1. Introduction

Aristolochic acids (AAs) are presented in Aristolochiaceae plants such as Aristolochia and Asarum and their products (Liu, Xian, et al. 2021). While AA-I is a kind of the most toxic aristolochic acid compounds (Chan et al. 2019). Long-term exposure to AAs easily leads to the destruction of kidney structure and function, the main clinical manifestation is acute renal tubular injury, and severe cases can develop into renal failure (Li et al. 2018). Renal injuries continue to worsen even after AAs are discontinued. In addition, AAs are genotoxic and carcinogenic to humans. It could induce injuries and tumors in the stomach, kidneys, renal pelvis, bladder, liver, and lungs of rats and mice (Li et al. 2020; Kocic et al. 2021; Wang et al.). The relevant survey results show that in the past few decades, the global AAN related cases had a growing trend (Jadot et al. 2017). However, due to the influence of various factors, its true incidence is not clear, and it is likely to be underestimated. Retrospective analysis of some patients with chronic renal injury, evidence also points to having taken "Chinese herbal medicines containing AAs" at a certain time (Lai et al. 2009). Some studies also found that AAs could be transferred to soil and the edible part of the plants, thus generating a certain risk of food pollution (Li, Hu, and Chan 2016; Chan et al. 2019; Gruia et al. 2018; Li et al. 2018; Pavlovic et al. 2013; Au et al. 2020; Lukinich-Gruia et al. 2022;

Draghia et al. 2021). No effective AAN treatment worldwide is confirmed worldwide, and there is no available standard remediation method for AA-contaminated soil clean-up. AAN is recognized as a global environmental and public health safety issue (Jelakovic et al. 2019).

Catalpol (CAT) is a functional food in China which belongs to iridoids and is one of Rehmannia glutinosa's key antioxidant active components (Zhang, Chen, and Li 2019; Bi et al. 2019). CAT has abundant biological properties, including hypoglycemic, antioxidant, anti-tumor, anti-osteoporosis, reducing muscular atrophy, boosting immunity, neuroprotection, and cardiovascular protection (Au et al. 2020; Bi et al. 2019; Xu et al. 2018; Xiong et al. 2017; Wang and Hu 2018; Wang et al. 2020; Liu, Kong, et al. 2021; Xu et al. 2021). Functioning as a guardian in various tissue or cell injuries such as liver (Liu et al. 2018), kidney (Zhang, Bi, et al. 2019), myocardium (Lin et al. 2017). Although CAT has a wide range of anti-disease and health care effects in edible and medicinal use, no scholar has found that CAT protects against AA-I-induced kidney damage and associated mechanisms. Therefore, this experiment mainly investigated whether CAT could alleviate AA-I-induced renal injury by regulating oxidative stress, inflammatory response, apoptosis, and fibrosis, to assess the potential preventive effects and application value of CAT, an active pharmacological component of Rehmannia glutinosa, on AAN.

2. Materials And Methods

2.1. Culture of NRK-52E Cells

Rat tubular epithelial cell line (NRK-52E cells) were bought from the National Collection of Authenticated Cell Cultures, and were seeded in the DMEM culture medium including 10% FBS, 100 U/mL streptomycin and cultured under the condition of 5% CO2 saturated humidity at 37°C.

2.2. Selection of Drug Concentration for NRK-52E Cells

Three duplicate wells in each batch of 96-well plates with such cells were were planted with density of 1×10^5/mL. Each well was treated for 24 h with AA-I or/and CAT at various doses, and then 10 μL of CCK-8 solution (meilunbio, Dalian, China) was added. And then incubated at 37°C for 2 h. By using a microplate reader, the absorbance (A) value at 450 nm was found to quantify the viability of the cells (Biotek, MQX200, Winooski, VT, USA).

2.3. Treatment and Morphological Observation of NRK-52E Cells

The grouping and treatment of NRK-52E cells are shown in Table 1. Before treatment with AA-I or/and CAT for 24 h, incubated in serum-free medium for 6 h. Morphological changes of the cells were observed by an optical microscope (Nikon, Tokyo, Japan).

Table 1
Experimental grouping and drug administration in vitro.

Group	Drug administration
Control group	DMSO
Model (AA-I) group	AA-I, 40 μM (DMSO)
CAT group	CAT, 10 μM (DMSO)
LC group	AA-I (40 μM) + CAT (5 μM) (DMSO)
HC group	AA-I (40 μM) + CAT (10 μM) (DMSO)
AA-I + ML385 group	AA-I (40 μM) + ML385 (5 μM) (DMSO)
AA-I + ML334 group	AA-I (40 μM) + ML334 (100 μM) (DMSO)
AA-I + CAT + ML385 group	AA-I (40 μM) + CAT (10 μM) + ML385 (5 μM) (DMSO)
AA-I + PDTC group	AA-I (40 μM) + PDTC (100 μM) (DMSO)

2.4. Ultrastructure of NRK-52E Cells with Transmission Electron Microscopy (TEM)

After the cell was treated based on the experimental groups, the culture medium was aspirated and digested with 0.25% trypsin. The cells were evenly blown and dispersed in 2.5% glutaraldehyde buffer and fixed in a refrigerator overnight at 4 °C, and then fixed in 1% osmic acid, dehydrated and replaced with ethanol and acetone. After embedding in Epon 812 embedding medium, and cutting into ultrathin sections of 50–60 nm under an ultramicrotome. After staining, the morphology of the cell was checked by TEM (Hitachi Limited, Tokyo, Japan).

2.5. Cell Apoptosis

After treating the cell according to the experimental groups, the culture medium was aspirated, digested with trypsin without EDTA, 1 ~ 5 × 10^5 cells were collected in each group. The flow cytometer was used to measure cell Apoptosis by Annexin V-FITC/PI Apoptosis Detection Kit (Bioss, Beijing, China) per the manufacturer's instructions.

2.6. Detection of Intracellular Reactive Oxygen Species (ROS) Level

The four groups of cells in the logarithmic growth phase were sown and cultivated in six-well plates for 24 h. Remove the cell culture medium by suction, and add appropriate volume of diluted (1:1000) DCFH-DA (meilunbio, Dalian, China) working solution. Incubate the cells under the conditions of 37°C for 30 min, protected from light, and then wash the cells with serum-free culture medium for 3 times. Fluorescence signals were measured by Image-Pro Plus software with the same parameters.

2.7. Detection of Intracellular Ca^{2+} Level

To analyze cytoplasmic calcium, cells were treated according to the grouping method. 1×10^6 NRK-52E cells were harvested and stained with Fura-2/AM (4 μM; AAT Bioquest, USA) for 50 min at 37 ℃. The fluorescence intensity of Ca2 + was observed by Biotek Synergy 1 fluorescence spectrophotometer (Synergy H1, BioTek, USA) with excitation wavelengths of 340 and 380 nm and emission at 510 nm.After 5 min, the fluorescence intensity ratio was R value, and then Triton X-100 with the final concentration of 0.1% was added to destroy the cell membrane. At this time, the maximum fluorescence ratio Rmax was measured. At 5 min, EGTA was added to make its final concentration 10 nM, and the minimum fluorescence ratio Rmin was determined. Under physiological conditions, K_d = 224 nM, and the unit of $[Ca^{2+}]$ i is nM. The formula of $[Ca^{2+}]$ i is as follows:

$$[Ca^{2+}]\ i = K_d \times (R - Rmin) / (Rmax - R)$$

2.8. Immunofluorescence (IF) Staining of NRK-52E Cells

After cells had been plated into 24-well plates, they were treated with AA-I (40 μM) or CAT (10 μM) for 24 h. Immunofluorescence (IF) Staining of NRK-52E Cells was performed as Wang (Wang et al. 2022).The primary antibodies were shown in Table 2, and the fluorescence signals were collected and quantified by Image-Pro Plus software with the same parameters.

Table 2
Antibodies and other reagents

Antibodies and reagents	Manufacturers
Antibodies for western blot	
Rabbit anti-Nrf2 (1:1000)	Bioss, Beijing, China
Rabbit anti-HO-1 (1:1000)	Bioss, Beijing, China
Rabbit anti-Keap-1 (1:1000)	Bioss, Beijing, China
Rabbit anti-NQO1 (1:1000)	Bioss, Beijing, China
Rabbit anti-NF-kB p65 (1:1000)	Bioss, Beijing, China
Rabbit anti-NF-kB p-p65 (1:1000)	ABclonal,Wuhan,China
Rabbit anti-Myd88 (1:1000)	Affinity, Jiangsu, China
Rabbit anti-Cytochrome C (1:1000)	Affinity, Jiangsu, China
Rabbit anti-pro-IL-1β (1:1000)	Affinity, Jiangsu, China
Rabbit anti-TNF-α (1:1000)	Wanleibio, Harbin, China
Rabbit anti-Bax (1:1000)	Affinity, Jiangsu, China
Rabbit anti- BcL-2 (1:1000)	Bioss, Beijing, China
Rabbit anti-Caspase 3 (1:1000)	Affinity, Jiangsu, China
Rabbit anti-Cleaved-Caspase 3 (1:1000)	Affinity, Jiangsu, China
Rabbit anti-Caspase 9 (1:1000)	Wanleibio, Harbin, China
Rabbit anti-Cleaved-Caspase 9 (1:1000)	Affinity, Jiangsu, China
Rabbit anti-TGF-β1 (1:1000)	Bioss, Beijing, China
Rabbit anti-Smad2 (1:1000)	Bioss, Beijing, China
Rabbit anti-Smad3 (1:1000)	Bioss, Beijing, China
Rabbit anti-Smad7 (1:1000)	Bioss, Beijing, China
Rabbit anti-TIMP-1 (1:500)	Wanleibio, Harbin, China
Rabbit and anti-MMP9 (1:1000)	Bioss, Beijing, China
Rabbit anti-β-actin (1:10000)	Bioss, Beijing, China
Rabbit anti-GAPDH (1:10000)	Bioss, Beijing, China

Antibodies and reagents	Manufacturers
Antibodies for Immunohistochemistry	Servicebio, Wuhan,China
Rabbit anti-Nrf2 (1:200)	Servicebio, Wuhan,China
Rabbit anti-NF-kB (1:400)	
Rabbit anti-TGF-β1 (1:200)	Servicebio, Wuhan,China
Rabbit anti -COL-I (1:200)	Servicebio, Wuhan,China
Rabbit anti -COL-III (1:200)	Servicebio, Wuhan,China
Rabbit anti-FN (1:200)	Servicebio, Wuhan,China
Rabbit anti-α-SMA (1:200)	Servicebio, Wuhan,China
Rabbit anti-E-cad (1:200)	Servicebio, Wuhan,China
Rabbit anti-CTGF (1:200)	Servicebio, Wuhan,China
Rabbit anti-CHOP (1:300)	Servicebio, Wuhan,China
Rabbit anti-GRP78 (1:300)	Servicebio, Wuhan,China
Antibodies for Immunofluorescence	Bioss, Beijing, China
Rabbit anti-Nrf2 (1:100)	Bioss, Beijing, China
Rabbit anti-NF-κB p65 (1:100)	ABclonal,Wuhan, China
Rabbit anti-NF-κB p-p65 (1:100)	Bioss, Beijing, China
Rabbit anti-TGF-β1 (1:100)	Servicebio, Wuhan,China
Rabbit anti -COL-I (1:100)	Servicebio, Wuhan,China
Rabbit anti -COL-III (1:100)	Servicebio, Wuhan,China
Rabbit anti-FN (1:100)	Servicebio, Wuhan,China
Rabbit anti-α-SMA (1:100)	Servicebio, Wuhan,China
Rabbit anti-E-cad (1:100)	Servicebio, Wuhan,China
Rabbit anti-CTGF (1:100)	Servicebio, Wuhan,China
Rabbit anti-CHOP (1:200)	Servicebio, Wuhan,China
Rabbit anti-GRP78 (1:200)	

Antibodies and reagents	Manufacturers
Aristolochic acid A (313-67-7)	Dasfbio, Nanjing, China
Catalpol (2415-24-9)	Dasfbio, Nanjing, China
ML385 (846557-71-9)	MCE,Shanghai,China
ML334 (1432500-66-7)	MCE,Shanghai,China
PDTC(5108-96-3)	MCE,Shanghai,China

2.9. Animal Experiments and Sample Collection

Chinese Liaoning Changsheng Biotechnology Co., Ltd. provided SPF C57BL/6NJ male mice aged 6 weeks (18 ~ 20 g). Feeding conditions were set at 21°C ~ 23°C, a relative humidity of 35% ~ 65%, and a light/dark cycle of natural daylight with free access to standard pellet feed and drinking water. 30 mice with similar body weights were randomly selected after 1 week of adaptive feeding. They are randomly divided into 5 groups as shown in Table 3. CAT (purity ≥ 95%, CAS No. 2415-24-9) and AA-I (purity ≥ 95%, CAS No. 313-67-7) selected 0.5% sodium methylcellulose solution (0.5% CMC) as the vehicle and were intragastrically administered to mice for 28 d. The AA-I reference dose was determined based on our preliminary experiments (Supplementary results). The mice were weighed and sedated with ether on the 29th day. The blood was taken from the retro-orbital venous plexus, centrifuged for 15 min at 1500 r/min at 4°C, subpackaged, and stored. The kidneys were dissected and weighed, some were fixed in 4% paraformaldehyde solution, and the other were cryopreserved at -80°C.

Table 3
Experimental grouping and drug administration in vivo.

Group	Drug administration
Control group	0.5% CMC
Model (AA-I) group	AA-I, 10 mg/kg·d (0.5% CMC)
CAT group	CAT, 100 mg/kg·d (0.5% CMC)
LC group	AA-I (10 mg/kg·d) + CAT (10 mg/kg·d) (0.5% CMC)
HC group	AA-I (10 mg/kg·d) + CAT (100 mg/kg·d) (0.5% CMC)

2.10. Assessment of Renal Function and Oxidative Stress

The concentration of BUN and Cr in the serum was determined using biochemical kits. Renal tissues were ground into tissue homogenates with phosphate buffer (w/v, 1:9), centrifuged at 3500 r/m for 15 min in 4°C, and protein samples were quantified using a biochemical kit. As oxidative stress was assessed, the

MDA content as well as the activities of GSH-Px, SOD and T-AOC in mice renal tissue was detected using commercial kits as instructed by the manufacturer (all the kits were provided by Nanjing Jiancheng Bioengineering Institute, China).

2.11. Detection of Inflammatory Factors and Kidney Injury Biomarkers by ELISA

The levels of IL-1, IL-6, and IL-12 in serum of mice and the levels of NGAL and KIM-1 in renal homogenates were measured by ELISA kits (Chenglin, Beijing, China) based on the relevant instructions.

2.12. Histopathological Analysis of Kidney

The renal tissues were respectively stained with H&E, Masson staining and periodic acid-Schiff staining (PAS) (Liu, Li, et al. 2021). An optical microscope was used for observations and picture capturing. Semiquantitative scoring was used to rate the tubular injury level (Rafiee et al. 2022), and renal tissue injury was inspected blindly and scored based on the percentage of injured tubules (Li et al. 2022): 0: no injury; 1: < 25%; 2:25% ~ 50%; 3:50% ~ 75%; 4: > 75%.

2.13. Immunohistochemical (IHC) Staining of Kidney

The paraffin sections were processed by deparaffinization, hydration, etc(Wang et al. 2022). DAB coloration and hematoxylin counterstaining were then conducted to observe the experimental results under an optical microscope. ImageJ software quantified the positive areas of IHC. The primary antibodies were shown in Table 2.

2.14. Western Blotting (WB) Analysis: in Vivo and in Vitro

Extraction of the total renal protein: 100 mg of renal tissue was added to 1 mL of precooled RIPA lysate and 10 μL of protease inhibitor ground into tissue homogenate, centrifuged at 12 000 r/m for 20 min at 4°C.

Extraction of total cellular protein: The cells were washed with precooled PBS for 1 ~ 2 times, blotted dry with filter paper, added with 150 μL of lysis solution (RIPA lysis solution: protease inhibitor = 50:1), lysed at 4 ℃ for 30 min, scraped off the cells with a cell scraper, collected, centrifuged at 12 000 r/m for 10 min with 4 ℃, and then the supernatant was taken.

The protein concentration was measured by the BCA kit (meilunbio, Dalian, China), and the protein concentration of each group was adjusted to the same with lysis solution. 6 × SDS PAGE loading buffer was added at a ratio of 5:1, denatured in a boiling water bath for 10 min, and stored at − 80°C. Protein samples were separated by polyacrylamide gel electrophoresis (concentration gel set at 80 V for 50 min and separation gel at 120 V, which was stopped when the indicator dye reached the bottom of the separation gel) after loading and transferred to PVDF membranes. PVDF membranes were blocked with 5% skim milk powder formulated in the TBST solution for 1.5 h at room temperature and washed 6 times on a horizontal shaker with TBST for 8 min each time; then primary antibodies (shown in Table 2) were

incubated overnight at 4°C. After these steps are completed, the membrane is washed. Then placed in goat anti-rabbit HRP at a dilution ratio of 1:5000, then incubated at 37°C for 1.5 h. After the film was rinsed, the chemiluminescent agent ECL was used to drop evenly on the membrane. The immunoreactive bands were exposed based on ECL reagents (Meilunbio, Dalian, China). Exposure was visualized by biological imaging system (Tanon, Shanghai, China). ImageJ software was used to analyze the relevant band intensities, and expression of proteins was normalized relative to β-actin or GAPDH.

2.15. RNA Extraction and qRT-PCR Analysis: in Vivo and in Vitro

Total RNA was extracted from renal tissues and NRK-52E cells by Trizol reagents (Invitrogen, Carlsbad, CA, USA) according to the manufacturer's instructions(Liu et al. 2022a). The concentration and purity of the extracted RNA were determined at 260/280 nm by spectrophotometer (Gene Quant 1300 GE, USA). The reverse transcribed RNA into cDNA using a commercial bio-RT highly sensitive first-strand cDNA synthesis kit. Amplification was performed in a Light Cycler R96 real-time PCR instrument (Roche, USA) using SYBR Green, High ROX (Bori Technology Co., Ltd., Hangzhou, China) reagent, and the relative mRNA levels were calculated according to the 2-ΔΔCt method. β-actin and GAPDH serve as endogenous controls for normalization. The genes tested and the corresponding primer sequences can be seen from Table 4.

Table 4
Sequences of oligonucleotide primers for qRT-PCR

Genes	Forward Primer	Reverse Primer
β-actin	5'-CTACCTCATGAAGATCCTGACC-3'	5'-CACAGCTTCTCTTTGATGTCAC-3'
GAPDH	5'-AGGTCGGTGTGAACGGATTTG-3'	5'-TGTAGACCATGTAGTTGAGGTCA-3'
Nrf2	5'-CAGCCATGACTGATTTAAGCAG-3'	5'- CAGCTGCTTGTTTTCGGTATTA-3'
Keap-1	5'-GACTGGGTCAAATACGACTGC-3'	5'-GAATATCTGCACCAGGTAGTCC-3'
HO-1	5'-TCCTTGTACCATATCTACACGG-3'	5'-GAGACGCTTTACATAGTGCTGT-3'
NQO1	5'-GAAGACATCATTCAACTACGCC-3'	5'-GAGATGACTCGGAAGGATACTG-3'
Caspase3	5'-GAAACTCTTCATCATTCAGGCC-3'	5'-GCGAGTGAGAATGTGCATAAAT-3'
Caspase9	5'-TGTGAATATCTTCAACGGGAGC-3'	5'-GAGTAGGACACAAGGATGTCAC – 3'
Cyt-c	5'-ATGCGGCCAAAAATGTGGTCTC-3'	5'-CTGCCAGAGGCGTCATAGTGTG – 3'
BAX	5'-TTGCCCTCTTCTACTTTGCTAG-3'	5'-CCATGATGGTTCTGATCAGCTC-3'
Bcl-2	5'-GATGACTTCTCTCGTCGCTAC-3'	5'-GAACTCAAAGAAGGCCACAATC-3'
MyD88	5'-TCATGTTCTCCATACCCTTGGT-3'	5'-AAACTGCGAGTGGGGTCAG-3'
NF-κB p65	5'-CACCAAGGATCCACCTCACC-3'	5'-CTCTATAGGAACTATGGATACTGCG-3'
TNF-α	5'-ATGTCTCAGCCTCTTCTCATTC-3'	5'-GCTTGTCACTCGAATTTTGAGA-3'
TGF-β1	5'-CCAGATCCTGTCCAAACTAAGG-3'	5'-CTCTTTAGCATAGTAGTCCGCT-3'
Smad2	5'-CTCTCCAACGTTAACCGAAATG-3'	5'-CACCTATGTAATACAAGCGCAC – 3'
Smad3	5'-ATTCCATTCCCGAGAACACTAA – 3'	5'-TAGGTCCAAGTTATTGTGTGCT-3'
Smad7	5'-CTGTGTTGCTGTGAATCTTACG-3'	5'-GAGACTCTAGTTCACAGAGTCG-3'
MMP9	5'-CAAAGACCTGAAAACCTCCAAC-3'	5'-GACTGCTTCTCTCCCATCATC-3'
TIMP-1	5'-GCAAAGAGCTTTCTCAAAGACC-3'	5'-CTCCAGTTTGCAAGGGATAGAT-3'

Table 5
English abbreviation

Abbreviations	Full Name	Abbreviations	Full Name
AAs	Aristolochic acids	E-cad	E-cadherin
AA-I	Aristolochic acid	FN	Fibronectin
AL-I	Aristolactam I	GSH-Px	Glutathione peroxidase
AAN	Aristolochic acid nephropathy	HO-1	Heme oxygenase-1
α-SMA	α-smooth muscle actin	KIM-1	Kidney injury molecule 1
CAT	Catalpol	Keap-1	kelch-like ECH-associated protein 1
CCK-8	Cell Counting Kit-8	MMP9	Matrix metalloproteinase 9
CMC	Carboxymethylcellulose sodium	MDA	Malondialdehyde
CTGF	Connective Tissue Growth Factor	MyD88	Myeloiddifferentiationfactor 88
Col-I	Collagen I	NGAL	Superoxide Dismutase
Col-	Collagen III	Nrf2	NF-E2-related factor 2
CTGF	Connective Tissue Growth Factor	NQO1	NAD(P)H quinone dehydrogenase 1
Col-I	Collagen I	NF-κB	Nuclear factor kappa-B
Col-	Collagen III	SOD	Malondialdehyde
DMEM	Dulbecco's modified eagle medium	Smad	Small Mothers Against Decapentaplegic
Cyt-c	Cytochrome C	TGF-β	Transforming growth factor-β
ECM	Extracellular matrix	T-AOC	Total antioxidant capacity
EMT	Epithelial-Mesenchymal Transition	TIMP-1	Tissue inhibitor of matrix metalloproteinase-1

2.16. Statistical Analysis

All experimental data were analyzed using ImageJ, Image-Pro Plus 6.0 (Media Cybernetics, Maryland, USA), Origin, Graphpad Prism8.4.0 (GraphPad Inc., La Jolla, USA). All results were repeated in at least three independent assays; and the data were expressed as mean ± standard deviation (mean ± SD, $n \geq 3$). Statistical significance analysis was analyzed based on ANOVA test and LSD test to check significant differences among the groups. Compared with the control group, * refer to $P < 0.05$, ** refer to $P < 0.01$, ***

refer to $P < 0.001$, **** refer to $P < 0.0001$; compared with the AA-I group, # refer to $P < 0.05$, ## refer to $P < 0.01$, ### refer to $P < 0.001$, #### refer to $P < 0.0001$.

3. Results

3.1. CAT maintains the vitality and morphology of NRK-52E cells exposed to AA-I.

No significant inhibitory effects on cell survival rate were observed with 0 ~ 5 μM AA-I administered after exposure for 24 h. The inhibitory effects on the viability of cells were obviously enhanced in a concentration-related style after AA-I increased to 10 μM. Cell viability was approximately 60% after the concentration of AA-I was 40 μM, which was suitable for subsequent assays (Fig. 1a). In addition, after the CAT was treated alone for 24 h, both 5 μM and 10 μM increased cell viability to some extent. However, after the CAT concentration reached 20 μM, NRK-52E cell viability was instead obviously reduced ($P < 0.05$) (Fig. 1b). After NRK-52E cells were treated with different concentrations of CAT in combination with AA-I (40 μM) for 24 h, both 5 μM CAT and 10 μM CAT could increase the NRK-52E cells viability significantly ($P < 0.01$) (Fig. 1c). The density of the control and CAT group was more moderate under the optical microscope and showed a homogeneous oval morphology. While after the 24 h of AA-I (40 μM) exposure, the cell density was significantly reduced and the morphology was irregular, and some cells were even detached. While in the AA-I + CAT intervention groups, the cell density was moderate, and irregular or detached cells were reduced compared with the AA-I group (Fig. 1d).

The above results reflect that AA-I (40 μM) exposure caused NRK-52E cytotoxic damage, and (5 μM and 10 μM) CAT was able to inhibit the toxic effects of NRK-52E cells exposed to AA-I.

3.2. CAT alleviates renal injury in AA-I model.

After 4 weeks of continuous administration in each group of test mice, no abnormalities occurred in the control and CAT group. Mice exposed to AA-I were thin and unresponsive, with rough, dull fur, and a low body temperature compared with the control group. Necropsy revealed that the kidneys of mice exposed to AA-I were slightly smaller in size and pale in color. Although the mental status of mice in the CAT intervention group (HC and LC) was not as good as the control group, the adverse reactions were relieved than the Model (AA-I) group. In addition, necropsy revealed that their kidneys were also less pale than those in the AA-I group.

The body weight of mice in the AA-I, LC and HC groups was significantly decreased compared with the control group ($P < 0.05$). No obvious differences existed in the CAT group ($P > 0.05$). The body weight of mice in the CAT and HC groups was significantly increased compared with the control group ($P < 0.05$). The body weight of mice in the LC group was slightly higher than that in the Model (AA-I) group, but without any significance ($P > 0.05$) (Fig. 2a).

Renal damage from AA-I exposure was evaluated based on measurements of BUN, Cr, NGAL, and KIM-1 in the serum (Fig. 2b, 2c, 2d, 2e). The BUN, Cr, NGAL and KIM-1 contents of CAT group mice and the NGAL contents of the LC and HC group mice did not change significantly compared with the control group ($P > 0.05$), but the BUN, Cr, NGAL and KIM-1 contents of Model (AA-I) group mice and the BUN, Cr, and KIM-1 contents of the LC and HC group mice were significantly increased ($P < 0.05$). The BUN, Cr and KIM-1 contents of the CAT, LC and HC groups mice, along with the NGAL contents in the CAT and HC groups, were reduced compared with the control group ($P < 0.05$).

It showed that AA-I could induce renal injury in mice, while CAT intervention could alleviate renal injury and body weight. The BUN, Cr, NGAL, and KIM-1 contents of mice in the high-dose CAT intervention group were recovered ($P < 0.05$).

3.3. CAT reduces the histopathological and cytological changes in AA-I model.

H&E staining (Fig. 3a) and PAS staining (Fig. 3b) reflected that the control group and the CAT group's renal tissue structure were intact, and no obvious pathological changes were found. Renal tubular epithelial cells were the most severely injured in mice with AA-I exposure, with vacuoles, pyknosis, shedding, nuclear dissolution, glomerular atrophy, and inflammatory cell infiltration in the renal interstitium. Tubular injury scores significantly increased (Fig. 3c). Although the renal damage of AA-I exposure was significantly reduced after CAT intervention, the corresponding pathological damage was not completely reversed. The ultrastructure of NRK-52E cells was checked by TEM (Fig. 3d). For the control group and CAT group, the organelle structure was intact and the mitochondrial contour was clear. No abnormality has been observed. While for the Model (AA-I) group, the cells showed nuclear membrane rupture, nuclear structure disassembly, organelle swelling, outer membrane damage in some mitochondria, disappearance of mitochondrial cristae, mitochondrial vacuoles and blurred matrix. The high-dose CAT (10 μM) intervention was able to significantly reduce the degree of AA-I-induced NRK-52E cell injury than the Model (AA-I) group. Moreover, the protective effect of CAT concentration of 10 μM better than 5 μM.

These results showed that CAT could inhibit the nephrotoxicity of AA-I exposure and alleviate the damage of renal tissue and tubular epithelial cells.

3.4. CAT reduces the oxidative stress damage of renal tissue and NRK-52E cells in AA-I model.

In vitro, we first verified the effects of CAT and AA-I on ROS content (Fig. 4a). It has been found that AA-I could increase the ROS levels in NRK-52E cells ($P < 0.01$). However, the ROS content was significantly decreased with CAT intervention ($P < 0.01$). After that, we assessed the effects of CAT and AA-I on oxidative stress status by measuring SOD, MDA, GSH-Px and T-AOC in vivo (Fig. 4b) and in vitro (Fig. 4c) by ELISA kits. Interestingly, both in vitro and in vivo showed a similar trend that AA-I exposure significantly decreased SOD, GSH-Px and T-AOC activities, but significantly increased MDA content

compared with the control group ($P < 0.01$). However, the high-dose CAT intervention could increase the SOD, GSH-Px and T-AOC activities significantly ($P < 0.01$). Furthermore, it effectively reversed the AA-I-induced increase in MDA content ($P < 0.01$). However, low-dose CAT intervention had no significant effects on oxidative stress parameters ($P > 0.05$). Combined with the results of transmission electron microscopy (Fig. 3d), the protective effects of low-dose CAT on NRK-52E cells were poor. Therefore, 10 μM CAT (AA-I + CAT group) was selected as the intervention dose for subsequent in vitro tests. By performing Nrf2 immunohistochemical staining in renal tissue (Fig. 4d) and immunofluorescence staining of Nrf2 in NRK-52E cells (Fig. 4e), we found that AA-I could reduce the expression of Nrf2 ($P < 0.01$), while CAT could increase it ($P < 0.01$). WB (Fig. 4f, 4h) and qRT-PCR (Fig. 4g, 4i) analysis revealed that the protein and gene expressions of Nrf2, Keap1, NQO1 and HO-1 in vitro were consistent with the trend in vivo, and the AA-I group obviously reduced these protein and gene expressions compared with the control group ($P < 0.05$). However, CAT could increase these protein and gene expressions, which AA-I-reduced ($P < 0.05$). In addition, in vivo experiments, the effects of high-dose CAT intervention were significantly better than that of the low-dose.

These results showed that CAT could down-regulate the over-expression of ROS in NRK-52E cells induced by AA-I exposure, and CAT had a protective effect on oxidative stress injury induced by AA-I.

3.5. CAT reduces the inflammatory injury of renal tissue and NRK-52E cells in AA-I model.

The IL-1, IL-6, and IL-12 level of renal tissue (Fig. 5a) and cells (Fig. 5b) were obviously increased in the AA-I group compared with the control group. CAT intervention could effectively reduce the contents of these inflammatory factors in renal tissue and cells of the AA-I group ($P < 0.05$). To research the effects of CAT and AA-I on the NF-κB signaling pathway, we first detected the expression of NF-κB by IHC staining (Fig. 5c) and IF staining (Fig. 5d). We found that AA-I was able to improve the NF-κB level in vivo and in vitro ($P < 0.01$). While CAT intervention could decline the increase of NF-κB expression induced by AA-I ($P < 0.01$). To further verify that CAT inhibited the inflammatory response induced by AAI through the NF-kB signaling pathway, the level of related factors and upstream and downstream products in renal tissue and NRK-52E cells were measured by WB (Fig. 5e, 5g) and qRT-PCR (Fig. 5f, 5h). The AA-I exposure significantly enhanced the level of MyD88, NF-κB p65, TNF-α compared with the control group ($P < 0.01$), while the CAT intervention could significantly decrease the expression of these proteins and genes ($P < 0.05$).

These results showed that AA-I activated the Myd88/NF-κB/TNF-α signaling pathway and released inflammatory factors such as IL-1, IL-6 and IL-12. Meanwhile, CAT attenuated these inflammatory responses induced by AA-I and played a protective role in renal tissue and tubular epithelial cells.

3.6. CAT reduces the apoptosis of renal tissue and NRK-52E cells in AA-I model.

The apoptosis (early and late) rate of cells cultured in vitro was detected by flow cytometry. The AA-I group's apoptosis rate was raised compared with the control group ($P < 0.01$). While CAT intervention could go down the apoptosis rate (Fig. 6a). The levels of CHOP, GRP78 and Ca^{2+} in cells (Fig. 6b, 6c) were determined by IF and Fluo-3, AM. It was found that AA-I could lead to a high up-grading in CHOP, GRP78, Ca^{2+} of NRK-52E cells ($P < 0.01$), while CAT intervention obviously reduced the level of CHOP, GRP78 and Ca2+ ($P < 0.01$). In addition, the relevant apoptotic proteins and genes in renal tissue and NRK-52E cells were detected by WB (Fig. 6d, 6f) and qRT-PCR (Fig. 6e, 6g). The results of the experiment reflect that the related indexes of Cyt-c, Bax, Cleaved Caspase-9/Caspase-9, Cleaved Caspase-3/Caspase-3 were increased, while Bcl-2 and Bcl-2/Bax were decreased in the AA-I group compared with the control group ($P < 0.05$), while CAT intervention obviously reversed these expressions ($P < 0.05$).

These results showed that CAT had an excellent protective effect on ER stress apoptosis and mitochondrial apoptosis induced by AA-I.

3.7. CAT reduces the oxidative stress, inflammation and apoptosis of NRK-52E cells induced by AA-I through regulating Nrf2/NF-κB system.

First, to verify whether CAT attenuated AA-I-induced oxidative stress and inflammatory injury through Nrf2/NF-κB, we performed nuclear translocation assays to inhibit and activate Nrf2 in vitro. Cell viability assays reflecting that ML385 decreased cell viability reached 46%, whereas ML334 and AA-I co-treatment increased cell viability to 78% (Fig. 7a). Compared with the control group, there was a decrease of Nrf2, and an increase of Myd88, NF-κB p65 and cleaved caspase-3 in the AA-I group ($P < 0.01$). But these changes were corrected by CAT ($P < 0.01$), this is the same as our previous results. But the improvement effect of CAT was obviously reduced or even ineffective after the ML385 was added. In contrast, AA-I-induced the decrease of Nrf2 and the increase of NF-κB p65, Myd88, cleaved caspase-3 were similarly corrected after ML334 was added (Fig. 7b, 7c). By immunofluorescence (Fig. 7d), we also concluded that CAT can activate nuclear translocation of Nrf2 and that Nrf2 negatively regulates NF-κB. To research the influence of CAT on NF-κB, this paper further performed inhibition assays on NF-κB in vitro. The cell viability was increased to 80% effect by co-treatment with PDTC and AA-I (Fig. 7e). Compared with the control group, the results reflected that NF-κB p-p65, pro-IL-1β, TNF-α and cleaved caspase-3 contents increased in the AA-I group, and the intervention of CAT and PDTC could obviously inhibit the high expression of these proteins induced by AA-I (Fig. 7f, 7g). Further, by immunofluorescence, we also verified that NF-κB/TNF-α pathways were positively correlated, and NF-κB was also the main target of CAT (Fig. 7h). These data demonstrate that both Nrf2 and NF-κB are the main targets of CAT to attenuate AA-I-induced renal injury. CAT could attenuate oxidative stress, inflammation and apoptosis induced by AA-I through the Nrf2/NF-κB system.

4. Discussion

To explore the protective function of CAT—the active component of the traditional drug Rehmannia glutinosa, on renal injury, we used C57BL/6N male mice as a model animal to establish an AAN model of

AA-I exposure. Renal function indicators such as SCr, BUN and renal injury markers such as KIM-1 and NGAL were significantly increased through clinical observation. Renal tubular scores decreased and many renal tubular epithelial cells were swollen or atrophied. Some renal tubules showed cast or structural destruction, and inflammatory cells and collagen fiber accumulation were observed in the interstitium. The results showed that AAN was successfully induced in C57BL/6N male mice with a dose of 10 mg/kg. The clinical symptoms of AAN mice were significantly alleviated with CAT intervention, and the renal function parameters and oxidative stress-related parameters were also significantly decreased, indicating that CAT has a therapeutic effect on ANN. Oxidative stress was considered as the main pathogenesis of AAN (Antoine et al. 2022; Zhang, ShiYang, et al. 2019; Liu et al. 2020). Therefore, we explored the protective mechanism of CAT on tubular epithelial cells based on the Nrf2/HO-1 antioxidant system. The expressions of IHC, IF, WB and qRT-PCR all demonstrated that the expression of Nrf2 could be significantly reduced by AA-I. While CAT intervention promoted the expression of Nrf2 and had a reversal effect on AA-I exposure-induced Nrf2 reduction. Normally, Nrf2 binds to Keap1 in cytoplasmic homeostasis. When oxidative stress occurs, Nrf2 is uncoupled with Keap1. Nrf2 also participated in the regulation of genes such as NQO1 and HO-1 (Chang et al. 2022). While NQO1 can prevent the adverse influence of quinones and their related compounds on tissues. HO-1 can improve the scavenging ability of cells for ROS and inhibit the production of pro-inflammatory mediators (Yachie 2021). As an upstream and downstream regulatory molecule, Nrf2/HO-1 is very crucial in anti-inflammatory and anti-oxidation(Liu et al. 2022b). It inhibits oxidative stress and inflammatory responses by activating the Nrf2/HO-1 system (Chen et al. 2021). This way can avoid the damage of tissue and cells caused by oxidative stress. Both studies in vivo and in vitro showed that AA-I obviously reduced the level of Nrf2, Keap1, HO-1 and NQO-1. While CAT up-regulated the Nrf2/HO-1 pathway, it enhanced the scavenging of ROS and reduced the oxidative stress induced by AA-I.

Nuclear factor kappa B (NF-κB), a vital transcription factor involved in signaling, regulates a variety of cellular processes, including infammatory processes (Zhu et al.). The NF-κB pathway is an intracellular signal transduction pathway sensitive to oxidative stress. When the body is stimulated by oxidative stress, NF-κB is activated through intracellular Myd88-dependent signal transduction pathways to release IL-1, IL-6, IL-12, TNF-α and ROS. These pro-inflammatory cytokines can further induce MyD88/NF-κB activation and cause oxidative stress. It has been shown that CAT can alleviate angiotensin II-induced renal injury by decreasing the levels of TNF-α and IL-6 (Cong et al. 2022). The results of this trial showed that AA-I was able to activate NF-κB and promote the over-expression of TNF-α, IL-1, IL-6 and IL-12, while CAT intervention alleviated this inflammatory response. It showed that CAT may inhibit the release of related inflammatory factors and the inflammatory response resulting from AA-I through the MyD88/NF-κB pathway. Apoptosis is a pathological response of the body against harmful stimuli. AA-I has been reported to trigger apoptosis by inducing mitochondrial dysfunction (Yang et al. 2019; Jin et al. 2020) and induced apoptosis based on the caspase3-dependent pathway (Li et al. 2010). In this experiment, we found that AA-I exposure could cause apoptosis phenomena in NRK-52E cells, such as nuclear fragmentation, organelle swelling, mitochondrial cristae breakage or mitochondrial disappearance. After CAT intervention, the corresponding abnormality was alleviated, and the cell activity was also improved.

The results of apoptosis rate also reflect these changes, which can play a certain mutual verification effect and improve the reliability of the results obtained. This study also found that AA-I exposure led to a significant reduction in Bax/Bcl2, and an increase in Cyt-c and the ratio of Cleaved Caspase-9/Caspase-9, Cleaved Caspase-3/Caspase-3. AA-I could cause intracellular ROS and Ca^{2+} accumulation in vitro, which could cause the over-expression of GRP78 and CHOP. While mitochondrial apoptosis and ER stress apoptosis affected by AA-I were restrained with CAT. The results were consistent with the fact that CAT could reverse triptolide-induced over-expression of Cleaved-Caspase3, Cleaved-Caspase9 and CHOP-mediated ER stress expression trend (Zhang et al. 2022).

These results suggest that CAT can inhibit AA-I nephrotoxicity by regulating oxidative stress, apoptosis and inflammatory response. These results also preliminarily suggest that Nrf2 and NF-κB are not parallel independent pathways, and there may be a relationship between them. We further used ML385 - a specific inhibitor of Nrf2 signaling pathway, and ML334-an activator of Nrf2 signaling pathway, to inhibit or activate Nrf2 signaling pathway and determine NF-κB signaling pathway and cleaved caspase-3 expression in AA-I-induced NRK-52E cells. We found that the Nrf2 signaling pathway negatively regulated NF-κB signaling pathway and caspase-3 was responsible for regulating apoptosis, and the effect of CAT on the Nrf2 signaling pathway was similar to that of the Nrf2 activator ML334. We also found the effect of CAT on the NF-κB signaling pathway was similar to that of PDTC. Exposure to AA-I breaks this balance system, causing an imbalance in oxidative stress and inflammatory responses, ultimately inducing and accelerating the progression of apoptosis. In total, the results of the above experiment reflected that ROS accumulated abundantly in NRK-52E cells induced by AA-I, increasing oxidative stress. AA-I induced decreased activity of the Nrf2 signaling pathway, resulting in decreased antioxidant function and inability to scavenge oxygen-free radicals in cells in a timely manner. Meanwhile, the pro-inflammatory signaling pathway NF-κB was activated. The combination of the two can accelerate the decline of cell vitality and induce apoptosis, while CAT can activate antioxidant function by regulating Nrf2/NF-κB system, reduce the level of inflammatory factors, inhibit cell apoptosis, and alleviate kidney damage. Next, we also need to deeply study whether CAT can regulate chronic renal anemia and renal fibrosis, and find out its mechanism.

5. Conclusions

In summary, AA-I can trigger oxidative stress and activate inflammatory reaction. It can further activate the mitochondrial pathway and ER stress pathway to induce apoptosis. CAT, as the main active ingredient of functional food Rehmannia glutinosa, can alleviate kidney injury by regulating Nrf2/NF-κB system, and its good antioxidant, anti-inflammatory and anti-apoptosis effects can be used as an effective candidate protective agent for preventing and treating renal injury (Figure 8).

Declarations

Availability of Data and Materials

The datasets used and/or analyzed during the current study are available from the corresponding author on reasonable request.

Consent for Publication

Written informed consent for publication was obtained from all participants.

Conflicts of Interest

All of the authors declare that they have no conflict of interest.

Acknowledgements

The authors thank Prof. Wenhui Yu for help in the experiments and Chinese Veterinary Research Institute of Northeast Agricultural University for facilities used in this study.

Funding

This work was supported by grants from the National Natural Science Foundation of China (32072909).

Ethics Declarations

The use of mice and all experimental protocols was approved by the Animal Ethics Committee of Northeast Agricultural University. All laboratory animals receive humane care according to the standards listed in the Guide for the Care and Use of Laboratory Animals (ISBN-10:1170-309-15396-4).

Author Contribution Statement

Zhihui Liu: Conceptualization, Methodology, Software, Investigation, Formal Analysis, Visualization, Writing - Original Draft; Yu Wang: Data Curation, Writing - Original Draft; Chong Zhou and Qingyang Xu: Visualization, Investigation; Hongxin Gao: Resources, Supervision; Mohan Huo: Software, Validation; Wenhui Yu and Xiaowen Jiang (Corresponding Author): Conceptualization, Funding Acquisition, Resources, Supervision, Writing - Review & Editing.

References

1. Antoine, M. H., C. Husson, T. Yankep, S. Mahria, V. Tagliatti, J. M. Colet, and J. Nortier. 2022. 'Protective Effect of Nebivolol against Oxidative Stress Induced by Aristolochic Acids in Endothelial Cells', Toxins, 14: 15.
2. Au, C. K., J. Y. Zhang, C. K. Chan, C. Li, G. R. Liu, N. M. Pavlovic, J. Yao, and W. Chan. 2020. 'Determination of Aristolochic Acids in Vegetables: Nephrotoxic and Carcinogenic Environmental Pollutants Contaminating a Broad Swath of the Food Supply and Driving Incidence of Balkan Endemic Nephropathy', Chemical Research in Toxicology, 33: 2446–54.

3. Bi, J. J., J. Li, S. J. Chen, J. K. Rao, Y. F. Xie, H. J. Yang, L. Wang, and B. F. Cheng. 2019. 'Catalpol ameliorates type II collagen-induced arthritis in rats and inhibits LPS-stimulated inflammatory response in SW982 human synovial cells', Journal of Functional Foods, 59: 291–300.
4. Chan, C. K., Y. S. Liu, N. M. Pavlovic, and W. Chan. 2019. 'Aristolochic Acids: Newly Identified Exposure Pathways of this Class of Environmental and Food-Borne Contaminants and its Potential Link to Chronic Kidney Diseases', *Toxics*, 7.
5. Chang, R. X., X. D. Sun, H. D. Jia, Q. S. Xu, Z. H. Dong, Y. Tang, S. B. Luo, Q. M. Jiang, J. J. Loor, and C. Xu. 2022. 'Inhibiting nuclear factor erythroid 2 related factor 2-mediated autophagy in bovine mammary epithelial cells induces oxidative stress in response to exogenous fatty acids', Journal of Animal Science and Biotechnology, 13: 11.
6. Chen, Y. Q., Y. Kong, Q. L. Wang, J. Chen, H. Chen, H. H. Xie, and L. Li. 2021. 'Schisandrin B Attenuates Airway Inflammation by Regulating the NF-kappa B/Nrf2 Signaling Pathway in Mouse Models of Asthma', *Journal of Immunology Research*, 2021: 13.
7. Cong, Cong, Xiaohong Yuan, Ying Hu, Wenjing Chen, Yong Wang, and Lei Tao. 2022. 'Catalpol Alleviates Ang II-Induced Renal Injury Through NF-kappaB Pathway and TGF-beta1/Smads Pathway', Journal of cardiovascular pharmacology, 79: e116-e21.
8. Draghia, L. P., A. T. Lukinich-Gruia, C. Oprean, N. M. Pavlovic, V. Paunescu, and C. A. Tatu. 2021. 'Aristolochic acid I: an investigation into the role of food crops contamination, as a potential natural exposure pathway', Environmental Geochemistry and Health, 43: 4163–78.
9. Gruia, A. T., C. Oprean, A. Ivan, A. Cean, M. Cristea, L. Draghia, R. Damiescu, N. M. Pavlovic, V. Paunescu, and C. A. Tatu. 2018. 'Balkan endemic nephropathy and aristolochic acid I: an investigation into the role of soil and soil organic matter contamination, as a potential natural exposure pathway', Environmental Geochemistry and Health, 40: 1437–48.
10. Jadot, I., A. E. Decleves, J. Nortier, and N. Caron. 2017. 'An Integrated View of Aristolochic Acid Nephropathy: Update of the Literature', International Journal of Molecular Sciences, 18.
11. Jelakovic, B., Z. Dika, V. M. Arlt, M. Stiborova, N. M. Pavlovic, J. Nikolic, J. M. Colet, J. L. Vanherweghem, and J. L. Nortier. 2019. 'Balkan Endemic Nephropathy and the Causative Role of Aristolochic Acid', *Seminars in Nephrology*, 39: 284 – 96.
12. Jin, C. N., X. Miao, Y. J. Zhong, J. H. Han, Q. Liu, J. C. Zhu, X. D. Xia, and X. L. Peng. 2020. 'The renoprotective effect of diosgenin on aristolochic acid I-induced renal injury in rats: impact on apoptosis, mitochondrial dynamics and autophagy', Food & Function, 11: 7456–67.
13. Kocic, G., M. Gajic, K. Tomovic, J. Hadzi-Djokic, M. Anderluh, and A. Smelcerovic. 2021. 'Purine adducts as a presumable missing link for aristolochic acid nephropathy-related cellular energy crisis, potential anti-fibrotic prevention and treatment', British Journal of Pharmacology, 178: 4411–27.
14. Lai, M. N., J. N. Lai, P. C. Chen, W. L. Tseng, Y. Y. Chen, J. S. Hwang, and J. D. Wang. 2009. 'Increased risks of chronic kidney disease associated with prescribed Chinese herbal products suspected to contain aristolochic acid', *Nephrology*, 14: 227 – 34.

15. Li, J., L. A. Zhang, Z. Z. Jiang, B. Shu, F. Li, Q. L. Bao, and L. Y. Zhang. 2010. 'Toxicities of aristolochic acid I and aristololactam I in cultured renal epithelial cells', Toxicology in Vitro, 24: 1092–97.
16. Li, W. W., C. K. Chan, Y. S. Liu, J. Yao, B. Mitic, E. N. Kostic, B. Milosavljevic, I. Davinic, W. H. Orem, C. A. Tatu, P. C. Dedon, N. M. Pavlovic, and W. Chan. 2018. 'Aristolochic Acids as Persistent Soil Pollutants: Determination of Risk for Human Exposure and Nephropathy from Plant Uptake', Journal of Agricultural and Food Chemistry, 66: 11468–76.
17. Li, W. W., Q. Hu, and W. Chan. 2016. 'Uptake and Accumulation of Nephrotoxic and Carcinogenic Aristolochic Acids in Food Crops Grown in Aristolochia clematitis-Contaminated Soil and Water', Journal of Agricultural and Food Chemistry, 64: 107–12.
18. Li, Xi-Lin, Xiao-Qing Guo, Hai-Rong Wang, Tao Chen, and Nan Mei. 2020. 'Aristolochic Acid-Induced Genotoxicity and Toxicogenomic Changes in Rodents', World journal of traditional Chinese medicine, 6: 12–25.
19. Li, Yanwei, Yuteng Jiang, Wei Zhou, Yiqian Wu, Shengnan Zhang, Guixia Ding, Yue Zhang, Aihua Zhang, Songming Huang, Zhanjun Jia, and Ran You. 2022. 'Maintaining homeostasis of mitochondria and endoplasmic reticulum with NSC228155 alleviates cisplatin-induced acute kidney injury', *Free radical biology & medicine*, 181: 270 – 87.
20. Lin, C., Y. Lu, X. J. Yan, X. Wu, M. Y. Kuai, X. Sun, Q. Chen, X. Y. Kong, Z. G. Liu, Y. P. Tang, Y. Jing, Y. Li, Q. C. Zhang, and H. M. Bian. 2017. 'Catalpol protects glucose-deprived rat embryonic cardiac cells by inducing mitophagy and modulating estrogen receptor', Biomedicine & Pharmacotherapy, 89: 973–82.
21. Liu, P. W., C. I. Li, K. C. Huang, C. S. Liu, H. L. Chen, C. C. Lee, Y. Y. Chiou, and R. J. Chen. 2021. '3-MCPD and glycidol coexposure induces systemic toxicity and synergistic nephrotoxicity via NLRP3 inflammasome activation, necroptosis, and autophagic cell death', Journal of Hazardous Materials, 405: 16.
22. Liu, S. L., Y. F. Kong, J. T. Cai, and C. H. Dong. 2021. 'Advances in Structural Modification and Pharmacological Activity of Catalpol and its Derivatives', Chemistryselect, 6: 13520–35.
23. Liu, S., Z. Xian, Y. Zhao, L. Wang, J. Tian, C. Pan, J. Han, Y. Zhang, C. Li, Y. Yi, C. Liu, D. Wang, J. Meng, S. Qin, F. Wang, and A. Liang. 2021. 'Quantitative Determination and Toxicity Evaluation of Aristolochic Acid Analogues in Asarum heterotropoides F. Schmidt (Xixin) and Traditional Chinese Patent Medicines', Front Pharmacol, 12: 761593.
24. Liu, X., J. Wu, J. Wang, X. Feng, H. Wu, R. Huang, J. Fan, X. Yu, and X. Yang. 2020. 'Mitochondrial dysfunction is involved in aristolochic acid I-induced apoptosis in renal proximal tubular epithelial cells', Human & Experimental Toxicology, 39: 673–82.
25. Liu, Z. G., P. T. Zhu, L. Zhang, B. Xiong, J. H. Tao, W. Guan, C. L. Li, C. Chen, J. Y. Gu, J. X. Duanmu, and W. Zhang. 2018. 'Autophagy inhibition attenuates the induction of anti-inflammatory effect of catalpol in liver fibrosis', Biomedicine & Pharmacotherapy, 103: 1262–71.
26. Liu, Zhihui, Bendong Shi, Yu Wang, Qingyang Xu, Hongxin Gao, Jun Ma, Xiaowen Jiang, and Wenhui Yu. 2022a. 'Curcumin alleviates aristolochic acid nephropathy based on SIRT1/Nrf2/HO-1 signaling

pathway', *Toxicology*, 479: 153297.

27. ———. 2022b. 'Curcumin alleviates aristolochic acid nephropathy based on SIRT1/Nrf2/HO-1 signaling pathway', *Toxicology*: 153297.
28. Lukinich-Gruia, Alexandra T., Joelle Nortier, Nikola M. Pavlovic, Dragan Milovanovic, Milos Popovic, Lavinia Paula Draghia, Virgil Paunescu, and Calin A. Tatu. 2022. 'Aristolochic acid I as an emerging biogenic contaminant involved in chronic kidney diseases: A comprehensive review on exposure pathways, environmental health issues and future challenges', *Chemosphere*, 297: 134111.
29. Pavlovic, N. M., V. Maksimovic, J. D. Maksimovic, W. H. Orem, C. A. Tatu, H. E. Lerch, J. E. Bunnell, E. N. Kostic, D. N. Szilagyi, and V. Paunescu. 2013. 'Possible health impacts of naturally occurring uptake of aristolochic acids by maize and cucumber roots: links to the etiology of endemic (Balkan) nephropathy (vol 35, pg 215, 2013)', Environmental Geochemistry and Health, 35: 417–17.
30. Rafiee, Zeinab, Mahmoud Orazizadeh, Fereshteh Nejad Dehbashi, Niloofar Neisi, Hossein Babaahmadi-Rezaei, and Esrafil Mansouri. 2022. 'Mesenchymal stem cells derived from the kidney can ameliorate diabetic nephropathy through the TGF-beta/Smad signaling pathway', *Environmental science and pollution research international*.
31. Wang, H. J., X. G. Xu, Y. Yin, S. Q. Yu, H. J. Ren, Q. Xue, and X. Y. Xu. 2020. 'Catalpol protects vascular structure and promotes angiogenesis in cerebral ischemic rats by targeting HIF-1 alpha/VEGF', *Phytomedicine*, 78: 14.
32. Wang, S., Z. H. Liu, Y. Wang, B. D. Shi, Y. Z. Jin, Y. Wang, X. W. Jiang, M. X. Song, and W. H. Yu. 'Grape seed extract proanthocyanidin antagonizes aristolochic acid I-induced liver injury in rats by activating PI3K-AKT pathway', Toxicology Mechanisms and Methods: 10.
33. Wang, Yu, Zhihui Liu, Jun Ma, Qingyang Xv, Hongxin Gao, Hang Yin, Ge Yan, Xiaowen Jiang, and Wenhui Yu. 2022. 'Lycopene attenuates the inflammation and apoptosis in aristolochic acid nephropathy by targeting the Nrf2 antioxidant system', Redox biology, 57: 102494.
34. Wang, Z. H., and Z. S. Hu. 2018. 'Catalpol inhibits migration and induces apoptosis in gastric cancer cells and in athymic nude mice', Biomedicine & Pharmacotherapy, 103: 1708–19.
35. Xiong, Y. J., L. Q. Shi, L. Wang, Z. J. Zhou, C. N. Wang, Y. Lin, D. Luo, J. J. Qiu, and D. P. Chen. 2017. 'Activation of sirtuin 1 by catalpol-induced down-regulation of microRNA-132 attenuates endoplasmic reticulum stress in colitis', Pharmacological Research, 123: 73–82.
36. Xu, D. Q., L. Wang, Z. Z. Jiang, G. L. Zhao, H. M. Hassan, L. X. Sun, S. S. Fan, Z. X. Zhou, L. Y. Zhang, and T. Wang. 2018. 'A new hypoglycemic mechanism of catalpol revealed by enhancing MyoD/MyoG-mediated myogenesis', Life Sciences, 209: 313–23.
37. Xu, D. Q., L. Zhao, S. J. Li, X. F. Huang, C. J. Li, L. X. Sun, X. H. Li, L. Y. Zhang, and Z. Z. Jiang. 2021. 'Catalpol counteracts the pathology in a mouse model of Duchenne muscular dystrophy by inhibiting the TGF-beta 1/TAK1 signaling pathway', Acta Pharmacologica Sinica, 42: 1080–89.
38. Yachie, A. 2021. 'Heme Oxygenase-1 Deficiency and Oxidative Stress: A Review of 9 Independent Human Cases and Animal Models', International Journal of Molecular Sciences, 22: 16.

39. Yang, X., D. Thorngren, Q. Chen, M. Wang, and X. C. Xie. 2019. 'Protective role of relaxin in a mouse model of aristolochic acid nephropathy', Biomedicine & Pharmacotherapy, 115: 7.
40. Zhang, J. N., R. Bi, Q. Meng, C. Y. Wang, X. K. Huo, Z. H. Liu, C. Wang, P. Y. Sun, H. J. Sun, X. D. Ma, J. J. Wu, and K. X. Liu. 2019. 'Catalpol alleviates adriamycin-induced nephropathy by activating the SIRT1 signalling pathway in vivo and in vitro', British Journal of Pharmacology, 176: 4558–73.
41. Zhang, L. L., C. Q. Li, L. Fu, Z. C. Yu, G. R. Xu, J. Zhou, M. Y. Shen, Z. Feng, H. X. Zhu, T. Xie, L. L. Zhou, and X. P. Zhou. 2022. 'Protection of catalpol against triptolide-induced hepatotoxicity by inhibiting excessive autophagy via the PERK-ATF4-CHOP pathway', *Peerj*, 10: 17.
42. Zhang, L. Q., K. X. Chen, and Y. M. Li. 2019. 'Bioactivities of Natural Catatpol Derivatives', Current Medicinal Chemistry, 26: 6149–73.
43. Zhang, Y., X. Y. ShiYang, Y. W. Zhang, Y. Li, X. Y. Shi, and B. Xiong. 2019. 'Exposure to aristolochic acid I compromises the maturational competency of porcine oocytes via oxidative stress-induced DNA damage', Aging-Us, 11: 2241–52.
44. Zhu, C., W. Chen, H. M. Cui, Z. G. Huang, R. Ding, N. Li, Q. Q. Wang, F. Wu, Y. M. Zhao, and X. L. Cong. 'TRIM64 promotes ox-LDL-induced foam cell formation, pyroptosis, and inflammation in THP-1-derived macrophages by activating a feedback loop with NF-kappa B via I kappa B alpha ubiquitination', Cell Biology and Toxicology: 14.

Figures

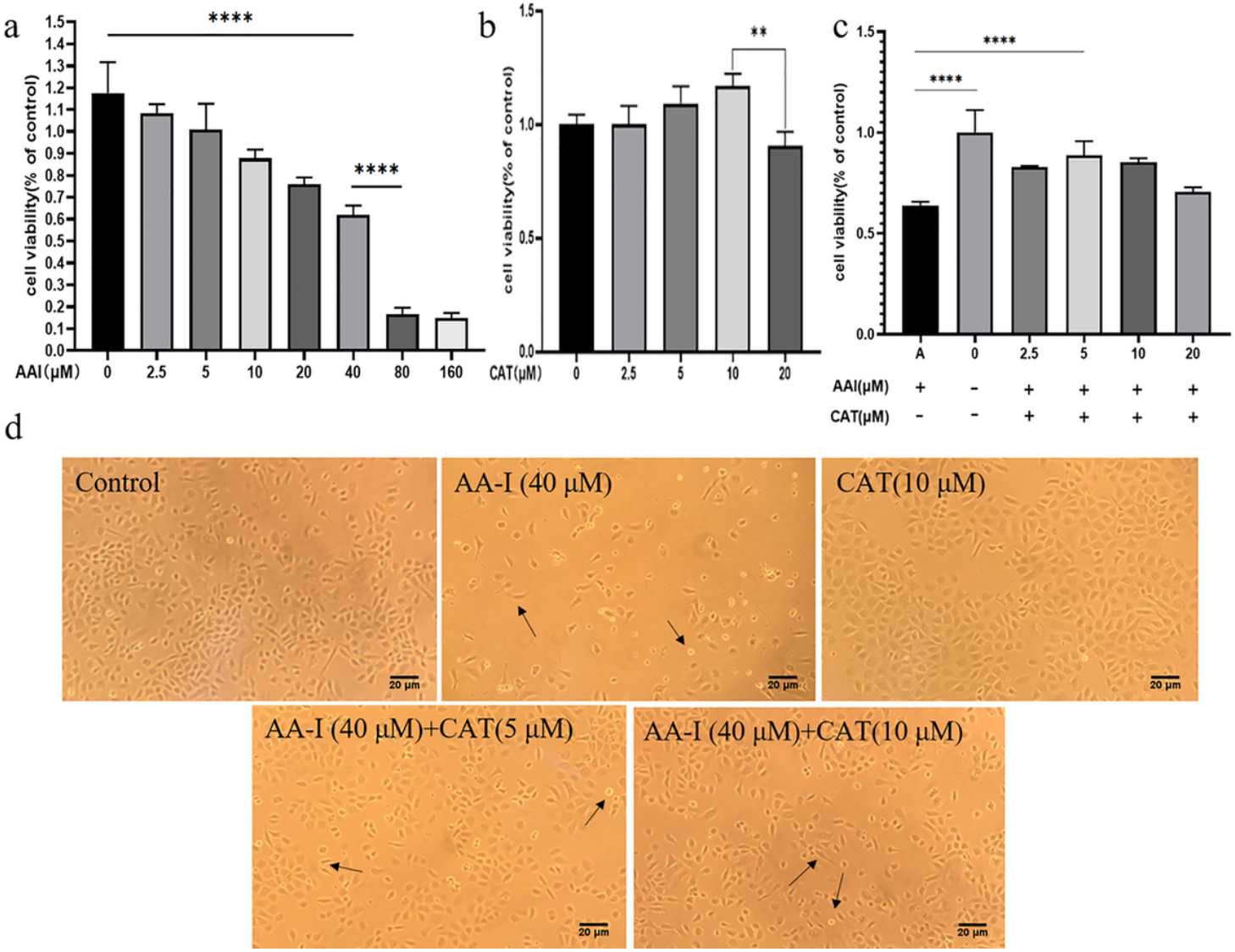

Figure 1

Effects of CAT intervention on the vitality and morphology of NRK-52 E cells exposed to AA-I (24h). In vitro, the cell viability of NRK-52E cells treated with 0 ~ 160 μM AA-I (a), 0~20 μM CAT (b) and 40 μM AA-I combined with 10 μ m or 5 μ m CAT (c) for 24 hours was measured by CCK-8 kit. The effects of two concentrations of CAT combined with 40 μM AA-I on the morphological changes of NRK-52E cells were observed by optical microscope (100 X) (d). Compared with the control group (mean ± SD, n ≥ 3) * refer to $P < 0.05$, ** refer to $P < 0.01$, *** refer to $P < 0.001$, **** refer to $P < 0.0001$; compared with the AA-I group, # refer to $P < 0.05$, ## refer to $P < 0.01$, ### refer to $P < 0.001$, #### refer to $P < 0.0001$.

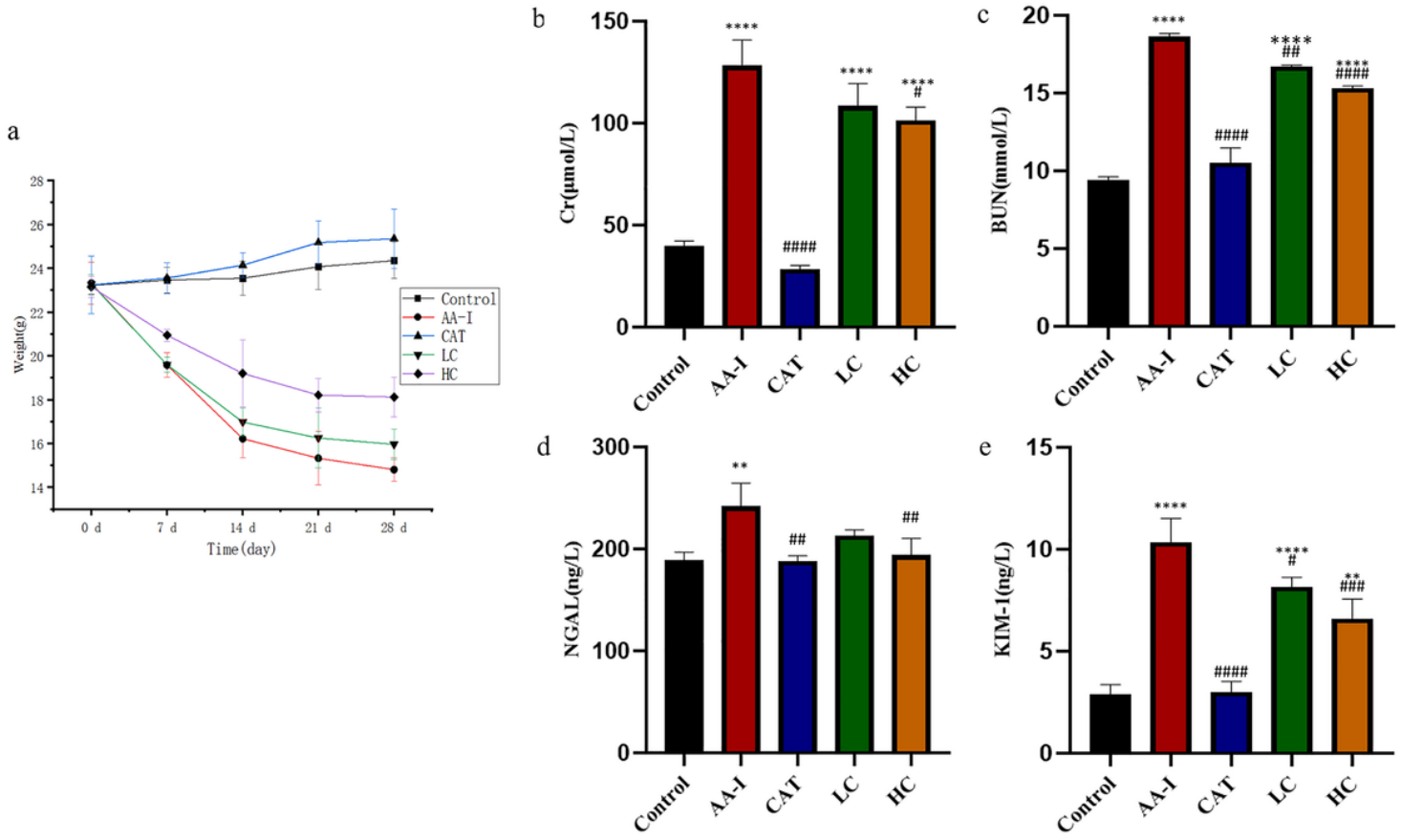

Figure 2

CAT alleviates the general condition and renal function in AA-I model. C57BL/6 male mice were exposed to AA-I (10 mg/kg) or/and intervened by CAT(100 mg/kg, 10 mg/kg) for 28 days. The body weight (a) was measured and the content of SCr (b), BUN (c), NGAL (d) and KIM-1 (e) were detected by Elisa. Compared with the control group (mean ± SD, n ≥ 3), * refer to $P < 0.05$, ** refer to $P < 0.01$, *** refer to $P < 0.001$, **** refer to $P < 0.0001$; compared with the AA-I group, # refer to $P < 0.05$, ## refer to $P < 0.01$, ### refer to $P < 0.001$, #### refer to $P < 0.0001$.

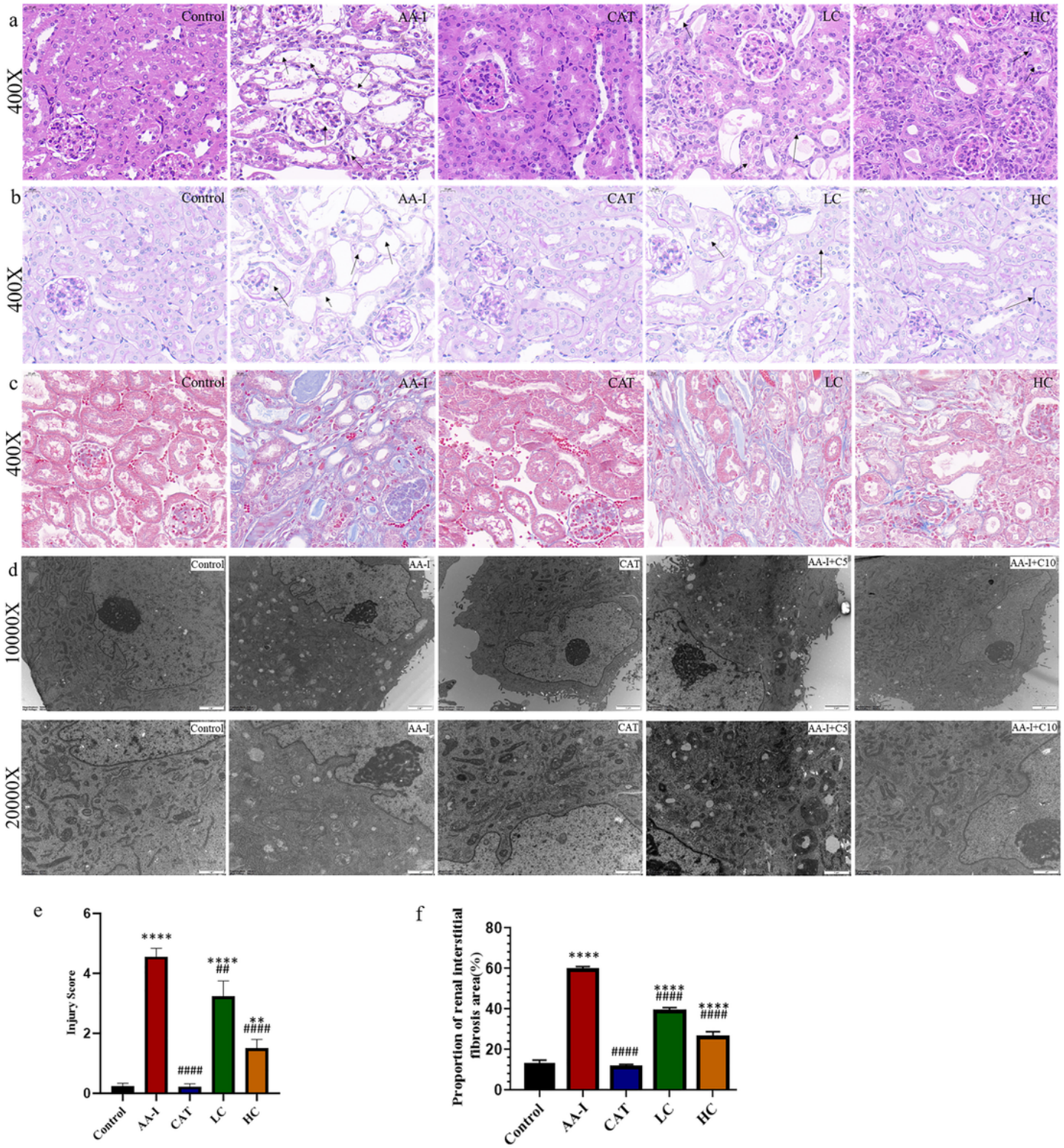

Figure 3

CAT reduces the histopathological and cytological changes in AA-I model. C57BL/6 male mice were exposed to AA-I (10 mg/kg) or/and intervened by CAT (100 mg/kg, 10 mg/kg) for 28 days. The renal tissue were stained with H&E (a) PAS (b) and Masson (c). The results of PAS were evaluated by renal tubular injury score (d). Ultrastructure of NRK-52E cells in each group (10 000 × and 20 000 ×) observed by transmission electron microscopy (e). Compared with the control group, * refer to $P < 0.05$, ** refer to P

< 0.01, *** refer to $P < 0.001$, **** refer to $P < 0.0001$; compared with the AA-I group, # refer to $P < 0.05$, ## refer to $P < 0.01$, ### refer to $P < 0.001$, #### refer to $P < 0.0001$.

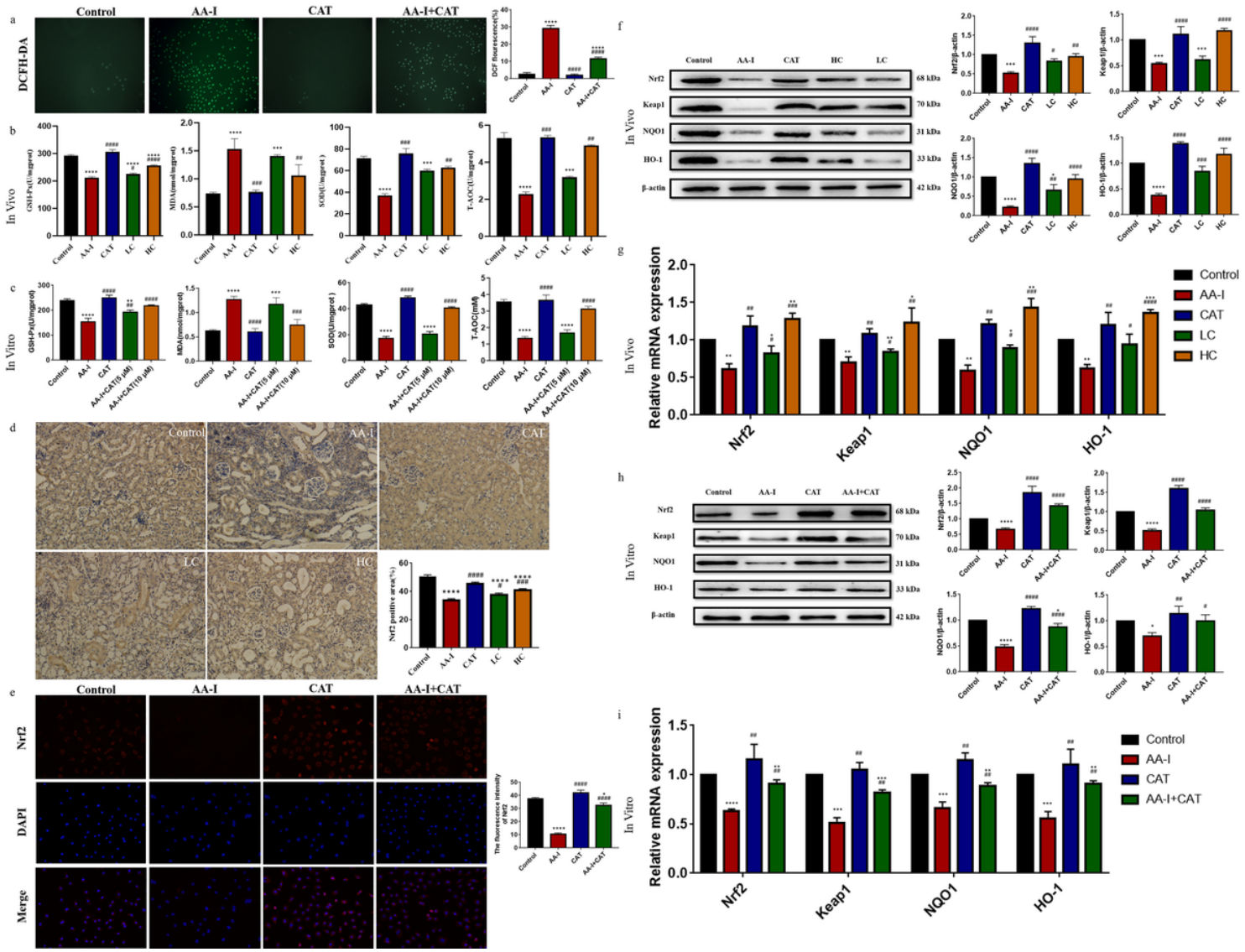

Figure 4

CAT reduces the oxidative stress damage of renal tissue and NRK-52E cells in AA-I model. In vitro, NRK-52E cells were exposed to AA-I (40μ m) or/and intervened by CAT (10 μM, 5 μM) for 24h. In vivo, C57BL/6 male mice were exposed to AA-I (10 mg/kg) or/and intervened by CAT (100 mg/kg, 10mg/kg) for 28 days. The ROS content in NRK-52E cells (a); oxidative stress index (b and c) was measured. And Nrf2 was measured by IHC (d) and IF (e). Western blot analyses and Quantitative RT-PCR assays were performed to detect Nrf2, Keap1, NQO1, and HO-1 protein (f and h) and mRNA (g and i) expression. Compared with the control group (mean ± SD, n ≥ 3), * refer to $P < 0.05$, ** refer to $P < 0.01$, *** refer to $P < 0.001$, **** refer to $P < 0.0001$; compared with the AA-I group, # refer to $P < 0.05$, ## refer to $P < 0.01$, ### refer to $P < 0.001$, #### refer to $P < 0.0001$.

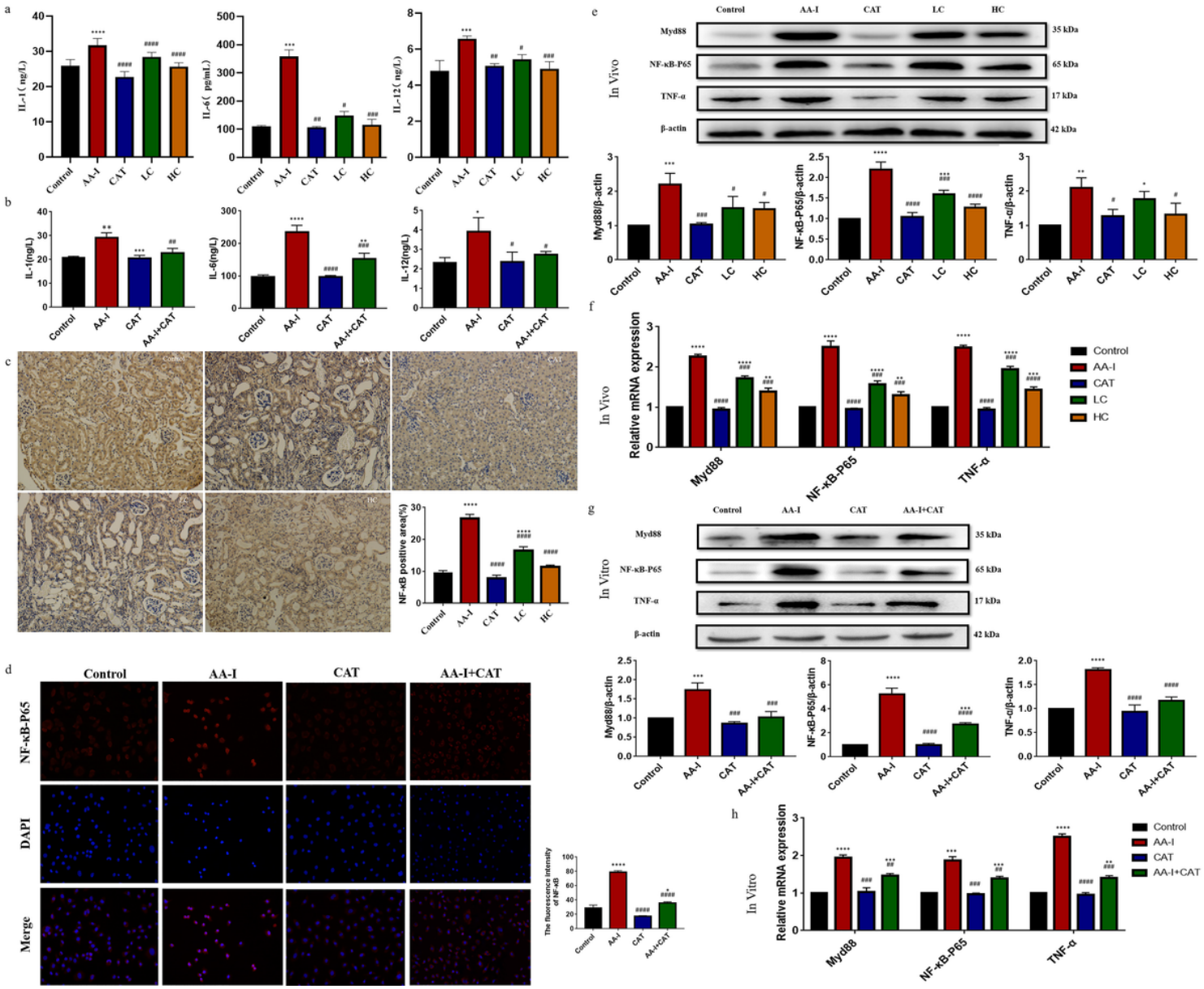

Figure 5

CAT reduces the inflammatory injury of renal tissue and NRK-52E cells in AA-I model. In vitro, NRK-52E cells were exposed to AA-I (40μ m) or/and intervened by CAT (10 μM, 5 μM) for 24h. In vivo, C57BL/6 male mice were exposed to AA-I (10 mg/kg) or/and intervened by CAT (100 mg/kg, 10mg/kg) for 28 days. IL-1, IL-6, and IL-12 content were measured by ELISA (a and b). And NF-κB was measured by IHC (c) and IF (d). Western blot analyses and Quantitative RT-PCR assays were performed to detect MyD88, NF-κB p65 and TNF-α protein (e and g) and mRNA (f and h) expression. Compared with the control group (mean ± SD, n ≥ 3), * refer to $P < 0.05$, ** refer to $P < 0.01$, *** refer to $P < 0.001$, **** refer to $P < 0.0001$; compared with the AA-I group, # refer to $P < 0.05$, ## refer to $P < 0.01$, ### refer to $P < 0.001$, #### refer to $P < 0.0001$.

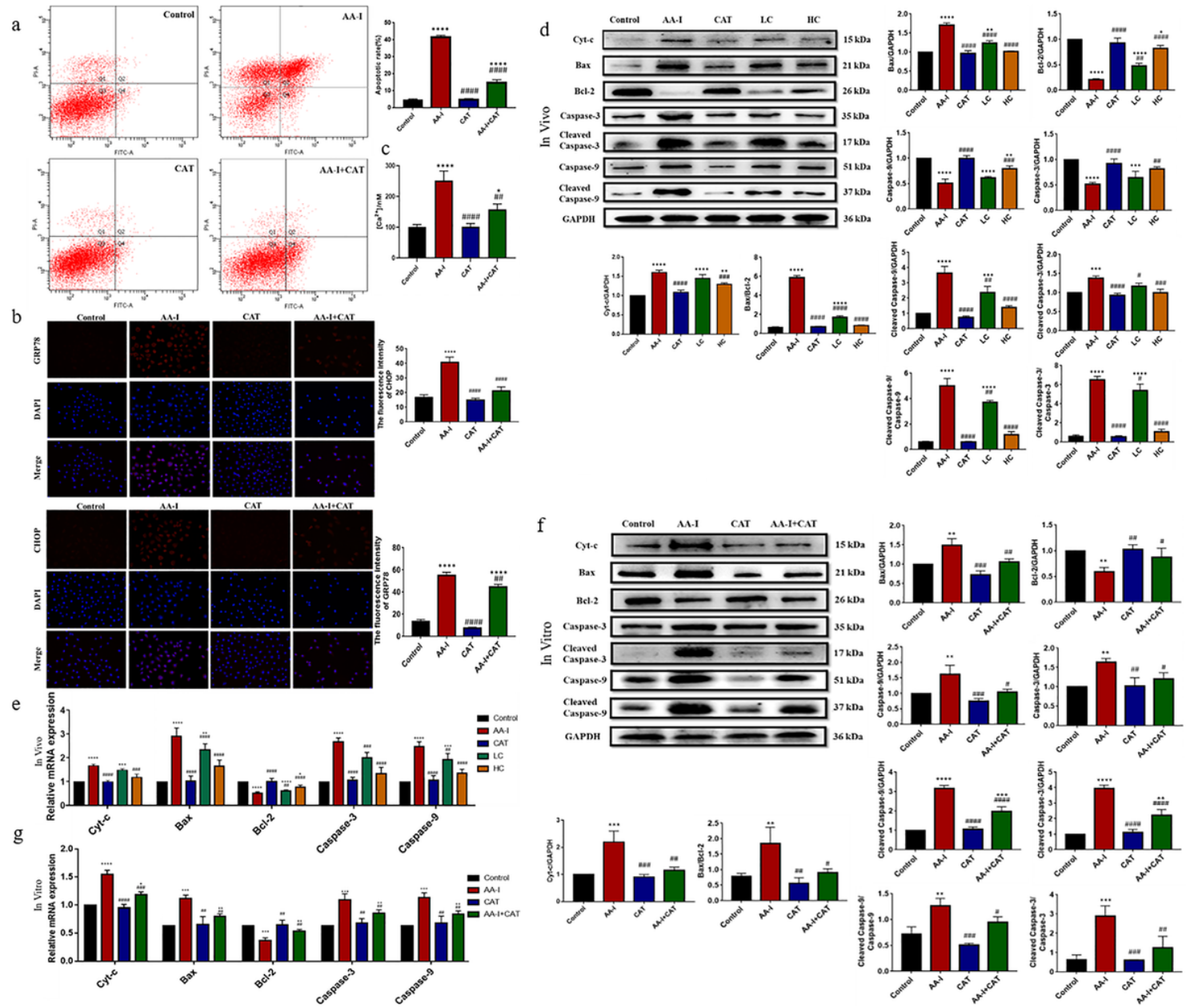

Figure 6

CAT reduces the apoptosis of renal tissue and NRK-52E cells in AA-I model. In vitro, NRK-52E cells were exposed to AA-I (40μ m) or/and intervened by CAT (10 μM, 5 μM) for 24h. In vivo, C57BL/6 male mice were exposed to AA-I (10 mg/kg) or/and intervened by CAT (100 mg/kg, 10mg/kg) for 28 days. Annexin V-FITC apoptosis detection kit was used to detect apoptosis by flow cytometry (a). GRP78 and CHOP were measured by IF (b) in NRK-52E cells. Ca^{2+} level was measured by fluorescence spectrophotometer in NRK-52E cells (c). Western blot analyses and Quantitative RT-PCR assays were performed to detect Cyt-c, Bax, Bcl-2, Caspase3, Cleaved-Caspase3, Caspase9, and Cleaved-Caspase9 protein (d and f) and mRNA (g and h) expression. Compared with the control group (mean ± SD, n ≥ 3), * refer to $P < 0.05$, ** refer to $P < 0.01$, *** refer to $P < 0.001$, **** refer to $P < 0.0001$; compared with the AA-I group, # refer to $P < 0.05$, ## refer to $P < 0.01$, ### refer to $P < 0.001$, #### refer to $P < 0.0001$.

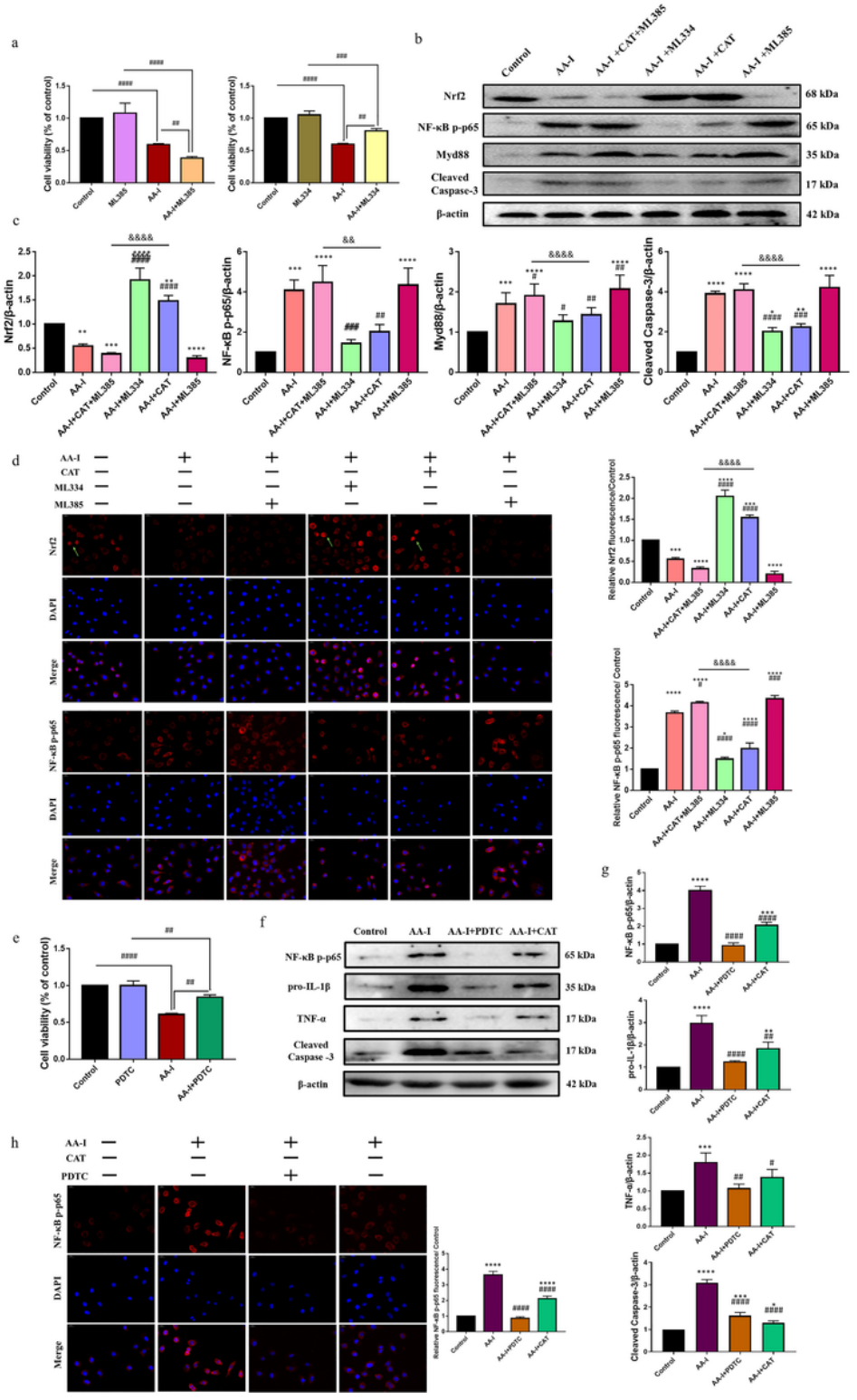

Figure 7

CAT reduces the oxidative stress, inflammation and apoptosis of NRK-52E cells induced by AA-I through regulating Nrf2/NF-κB system. NRK-52E cells were incubated with AA-I (40 μM) and treated with PDTC (100 μM) or CAT (20 μM) for 24 hours. Then cell viability was measured by CCK8 assay(a and e). Western blot assays were performed to detect Nrf2, NF-κB p-p65, Myd88 and Cleaved Caspase-3 expression (b and c). (d and h) Nrf2 and NF-κB p-p65 were measured by IF ("Green arrow" indicating the nuclear

translocation of Nrf2). NF-κB p-p65, pro-IL-1β and Cleaved Caspase-3 protein expression were measured by Western blot (f and g). Compared with the control group (mean ± SD, n ≥ 3), * refer to $P < 0.05$, ** refer to $P < 0.01$, *** refer to $P < 0.001$, **** refer to $P < 0.0001$; compared with the AA-I group, # refer to $P < 0.05$, ## refer to $P < 0.01$, ### refer to $P < 0.001$, #### refer to $P < 0.0001$.

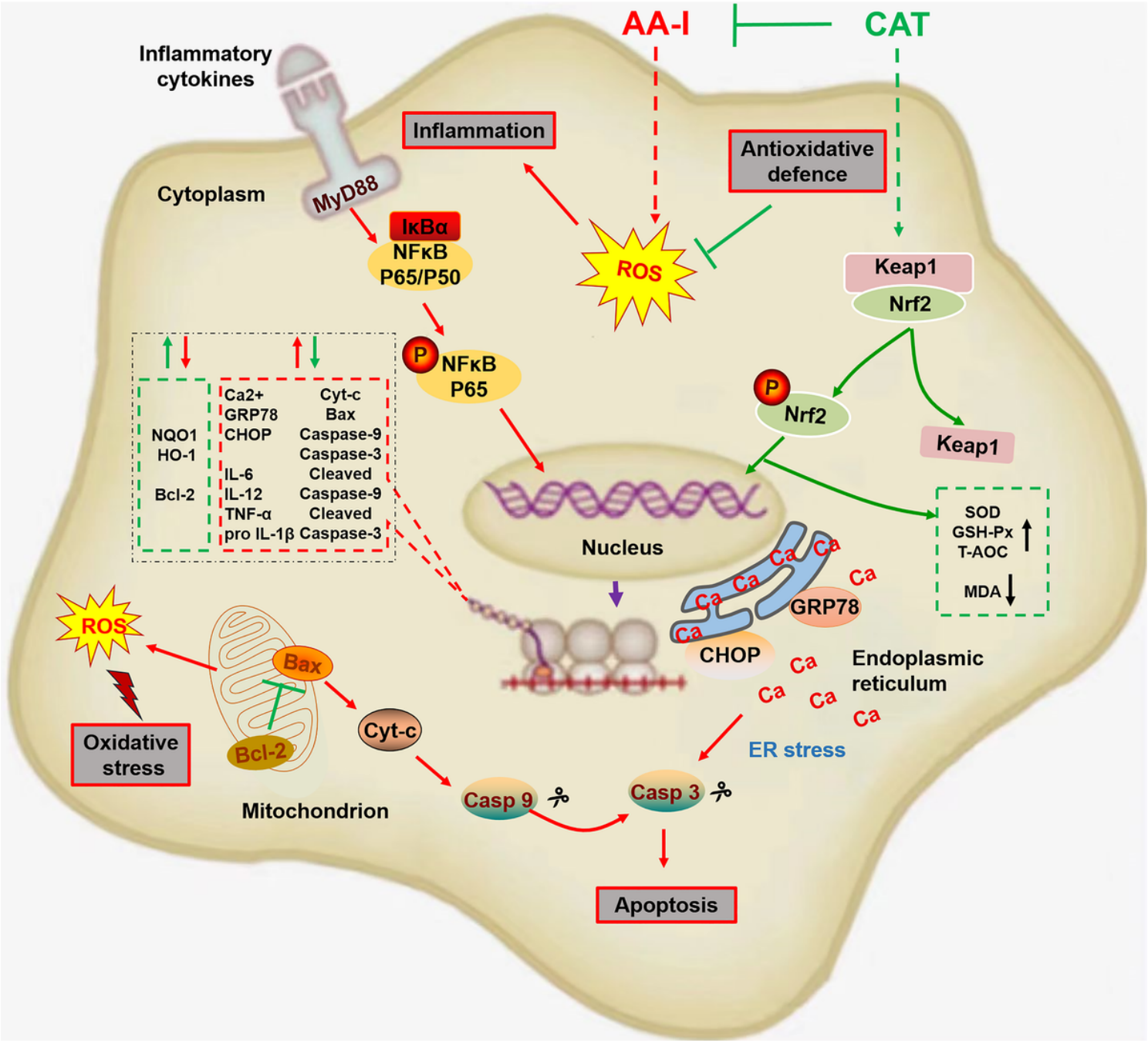

Figure 8

Schematic diagram of the mechanism by which CATalleviates AAN.

Supplementary Files

This is a list of supplementary files associated with this preprint. Click to download.

- AbstractpictureCAT1.tif
- SupplementaryResultCATAAI.docx